

## **Orientation relationship of Widmannstätten plates in an iron meteorite measured with high-energy synchrotron radiation**

**Hans Joachim Bunge, Wolfgang Weiss, Helmut Klein, Leszek Wcislak, Ulf Garbe and Jochen Richard Schneider**

Copyright © International Union of Crystallography

Author(s) of this paper may load this reprint on their own web site provided that this cover page is retained. Republication of this article or its storage in electronic databases or the like is not permitted without prior permission in writing from the IUCr.

# Orientation relationship of Widmannstätten plates in an iron meteorite measured with high-energy synchrotron radiation

Hans Joachim Bunge,<sup>a\*</sup> Wolfgang Weiss,<sup>b</sup> Helmut Klein,<sup>c</sup> Leszek Wcislak,<sup>d</sup> Ulf Garbe<sup>d</sup> and Jochen Richard Schneider<sup>d</sup>

<sup>a</sup>Department of Physics and Physical Technologies, Technical University of Clausthal, Leibniz Strasse 4, D-38678 Clausthal-Zellerfeld, Germany, <sup>b</sup>Gerstenkamp 9, D-51061 Köln, Germany, <sup>c</sup>Department of Mineralogy and Crystallography, University of Göttingen, Goldschmiedt Strasse 1, D-37077 Göttingen, Germany, and <sup>d</sup>Hamburger Synchrotronstrahlungslabor HASYLAB at Deutsches Elektronen-Synchrotron DESY, Notke Strasse 85, D-22603 Hamburg, Germany. Correspondence e-mail: hans.bunge@t-online.de

The orientation distribution of the Widmannstätten plates was measured in a sample of the Gibeon iron–nickel meteorite. The measurements were made with high-energy synchrotron radiation at beamline BW5 at HASYLAB/DESY in Hamburg using a high-resolution ‘moving-detector’ technique. The measurements reveal a continuous range of orientations stretching out from both sides of the Nishiyama–Wassermann orientation to the Kurdjumov–Sachs orientations, as well as a minor ‘spread-pipe’ between the Kurdjumov–Sachs ends of neighbouring non-coplanar orientation variants.

## 1. Introduction

Iron–nickel meteorites often show a well developed pattern of intersecting plates, observed for the first time by Widmannstätten (see *e.g.* Mehl, 1963). Different metallographic sections through such meteorites show that the plates are parallel to the side planes of an octahedron, for which reason these meteorites are called ‘octahedrites’. The plates consist of kamacite ( $\alpha$ -iron–nickel) and they are essentially monocrystals having a crystallographic  $\{110\}_\alpha$  plane parallel to the plane of the plate. It is now generally assumed that the plates were formed by a solid-state phase transformation from a monocrystalline region of taenite ( $\gamma$ -iron–nickel) when the material cooled extremely slowly (in space), with cooling rates of the order of 1 K per million years. Nucleation and growth of the kamacite crystals is assumed to be strictly crystallographically related to the crystal lattice of taenite in which they grow. Hence, the kamacite plates should have a definite crystallographic orientation relationship with respect to the original  $\gamma$  crystal. This assumption is corroborated by thin taenite ‘rims’, observed between the kamacite plates, which conserve the orientation of the original  $\gamma$  crystal.

The orientation relationship between  $\alpha$  and  $\gamma$  iron is usually expressed in terms of crystallographic planes and directions which are parallel to each other in the two crystal lattices. It is generally agreed that a  $\{110\}_\alpha$  plane is always parallel to a  $\{111\}_\gamma$  plane. There are, however, at least two different assumptions as to which directions in these two planes are parallel to each other. These were forwarded by Kurdjumov & Sachs (1930) (KS) on the one hand and by Nishiyama (1934) and Wassermann (1935) (NW) on the other hand. According to these assumptions:

$$\{110\}_\alpha \parallel \{111\}_\gamma; \begin{array}{l} \langle 111 \rangle_\alpha \parallel \langle 110 \rangle_\gamma \quad \text{KS} \\ \langle 110 \rangle_\alpha \parallel \langle 112 \rangle_\gamma \quad \text{NW} \end{array} \quad (1)$$

These two relationships seem to be very different, but, in fact, they are only 5.23° apart from each other.

The  $\gamma \rightarrow \alpha$  transformation plays an important role in the metallurgy of iron and steel. Hence, there is a very broad literature attempting to verify one or the other of these two relationships, as well as proposing crystallographic models which lead to either of them (see *e.g.* Haasen, 1974). It is assumed that any crystallographic relationship in a diffusive solid-state transformation is more precisely adhered to the closer to thermal equilibrium the transformation takes place. Hence, meteorites must be considered as unsurpassed samples in order to study this question.

Höfler *et al.* (1988) studied a sample of an octahedritic iron–nickel meteorite of the Gibeon shower by neutron diffraction. They came to the conclusion that both relationships of equation (1) must be assumed to be simultaneously valid. They further surmised that all intermediate relationships between the two are also possible. The neutron diffraction technique of Höfler *et al.* (1988) used step scans of the order of 1° × 2.5°. Hence, the angular resolving power of this measurement was not much higher than the distance between the two relationships and it was thus not sufficient to prove experimentally the hypothesis of a continuous transition between the two limiting relationships.

Much higher angular resolution can be reached with synchrotron radiation. In order to obtain, at the same time, a good statistical relevance, comparable with that of neutron diffraction, the radiation employed should have a penetration

depth that is larger than the size of the kamacite plates, as is in the iron–nickel case with neutron diffraction. This requires high-energy synchrotron radiation of  $\sim 100$  keV photon energy, corresponding to  $\sim 0.1$  Å wavelength.

In the present paper, we describe investigations of the orientation distribution of kamacite plates with the high-energy synchrotron texture diffractometer BW5 at HASYLAB (Wcislak *et al.*, 2002). The required high orientation resolution was achieved by a ‘moving-detector’ technique (Bunge *et al.*, 2002).

## 2. The experimental technique

The experimental technique is illustrated schematically in Fig. 1. A monochromatic X-ray beam of  $\sim 0.1$  Å wavelength and  $\sim 1 \times 1$  mm cross section falls onto the sample. It is diffracted in the angular range of  $2\theta \simeq 4^\circ$  into a set of Debye–Scherrer cones, which are registered on an area detector at a distance of  $\sim 1$  m from the sample. A Bragg-angle slit between sample and detector allows only one sector of one reflection ( $hkl$ ) at a time to reach the detector. The sample is then rotated continuously through the angle  $\omega$ , while, at the same time, the detector is shifted in the direction  $y$ . In this way, lattice planes ( $hkl$ ) with normal directions at the angles  $\{\omega\gamma\}$  come into reflection position and their orientation density is continuously imaged on the detector (Bunge *et al.*, 2002). Exposure times for the angular range  $-80 \leq \omega \leq 80^\circ$  are of the order of 10 min. In order for the X-ray beam to sweep over a sample volume containing a statistically relevant number of kamacite plates, the sample is also translated rapidly in the direction  $\pm y_s$  during exposure. The intensity registered in the pixels of the detector is colour-coded (as is shown later in Fig. 3). The density distribution in the resulting figure is equivalent to the conventional pole density distribution functions (pole figures) which are, however, usually represented in spherical polar coordinates  $\{\alpha\beta\}$  (see *e.g.* Wassermann & Grewen, 1962). The coordinate transformation between  $\{\omega\gamma\}$  and  $\{\alpha\beta\}$  is given, for instance, by Wcislak *et al.* (2002).

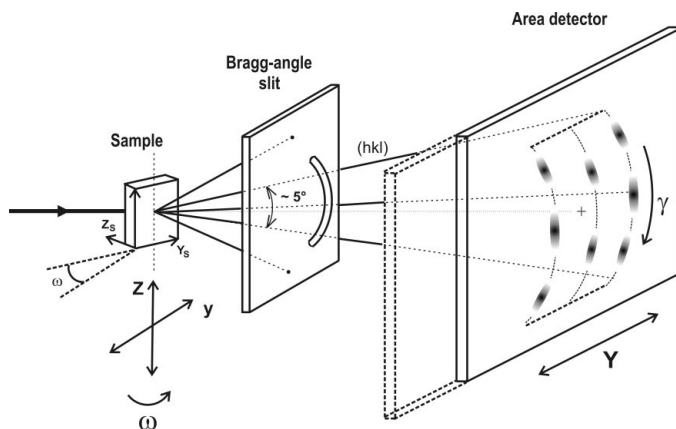


**Figure 1** Schematic view of the experimental diffraction installation at the beamline BW5 at DESY/HASYLAB in Hamburg, with the ‘moving-detector’ technique.

The angular resolving power of this technique is limited by the ‘pole-figure window’, *i.e.* the solid angular range which the instrument ‘sees’ in a fixed sample orientation, and the pixel size of the detector (Moras *et al.*, 2000). Because of the small wavelength, of the order of  $\sim 0.1$  Å, the pole-figure window is extremely anisotropic, *e.g.*  $0.025^\circ \times 1^\circ$  in the diffraction plane respectively perpendicular to it (Wcislak *et al.*, 2002). Hence, the angular resolving power in Fig. 3 is also different in different directions and it depends on the orientation angle  $\gamma$ . In the vicinity of the  $\{111\}$  poles in Fig. 3, it may be estimated as of the order of  $0.1^\circ$ .

## 3. The material and experimental results

The investigated sample was taken from a 28 kg specimen of the Gibeon meteorite shower (see *e.g.* Buchwald, 1975). Its Ni content was 7.93 wt%. The specimen was provided by the Mineralogical Museum of the University of Cologne. It belongs to the class of ‘fine octahedrites’, in particular to the group IV-A (see *e.g.* Heide & Wlotzka, 1995). A slice of 12 mm thickness was cut out of this sample with its plane nearly (but not exactly) parallel to the (001) plane of the original  $\gamma$  crystal. This slice was studied by optical metallography and by X-ray radiography (Weiss & Bunge, 2001). Fig. 2 shows an area of the optical micrograph. One can see traces of the kamacite plates along the  $[110]_\gamma$  and  $[\bar{1}\bar{1}0]_\gamma$  directions.

For X-ray diffraction according to Fig. 1, a smaller sample of  $10 \times 10 \times 1$  mm was cut out of the large one with its axes parallel to the cubic axes  $\langle 100 \rangle_\gamma$ . Fig. 3 shows the distribution of  $\langle 110 \rangle_\alpha$  crystal directions, *i.e.* the  $\langle 110 \rangle_\alpha$  pole figure. The figure shows the expected cubic symmetry of the original  $\gamma$  crystal (represented in the coordinates  $\{\omega\gamma\}$ ). One can clearly see the  $\{110\}_\alpha$  planes parallel to the four  $\{111\}_\gamma$  planes according to the left-hand side of the two orientation relationships of equation (1). Around these there are long stretches of intensity, as is to be expected according to the

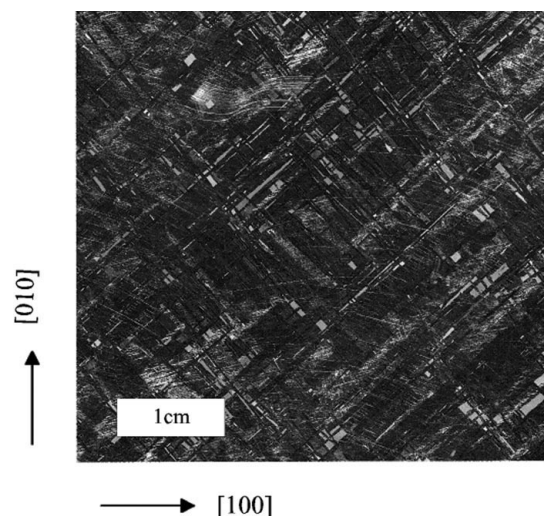


**Figure 2** Metallographic section of a slice of a specimen of the Gibeon meteorite cut (nearly) parallel to the (001) $_\gamma$  plane. It shows traces of Widmannstätten plates parallel to two  $\langle 110 \rangle_\gamma$  directions.

assumption of a continuous transition between the Kurdjumov–Sachs and the Nishiyama–Wassermann relationship. One can also see several stray intensity peaks, which may be attributed to kamacite crystals in the *plissit* regions, which are mixtures of non-oriented  $\alpha$  and  $\gamma$  crystals. Another intensity distribution with fourfold symmetry is seen around the  $[001]_\gamma$  pole.

#### 4. Discussion

Fig. 4(a) shows the  $\langle 110 \rangle_\alpha$  directions of kamacite crystals according to the relationship equation (1) with respect to the original  $\gamma$  crystal (taenite), projected onto the  $(111)_\gamma$  plane. One of the symmetrically equivalent variants of equation (1) is shown by bold lines. It is assumed that the orientations fill the range between two neighbouring KS orientations, *i.e.*  $KS_L$  and  $KS_R$ , continuously. The middle of this range is the NW orientation. Fig. 4(a) shows also the two other variants (labelled 2 and 3) with the same plane relationship [left-hand side of equation (1)] as the bold variant labelled 1. Furthermore, it shows the variants according to the other  $\{111\}_\gamma$  planes. It is seen that the  $\langle 110 \rangle_\alpha$  directions of three respective pairs of coplanar variants close up exactly to each other, thus forming three ‘double ranges’ (1–2, 2–3, 1–3) on the circle  $60^\circ$  from the central  $\langle 110 \rangle_\alpha$  direction.

Since Fig. 3 was taken with the sample in  $(001)_\gamma$  orientation, Fig. 4(a) was rotated to this orientation also, as shown in Fig. 4(b). The dashed circle in this figure shows the area visible in Fig. 3. Finally, the polar coordinates  $\{\alpha\beta\}$  of Fig. 4(b) were transformed into the experimental coordinates  $\{\omega\gamma\}$ , using the transformation relationship given by Wcislak *et al.* (2002), as shown in Fig. 4(c). This figure represents quite well the features of Fig. 3 [taking into account a slight deviation of the latter from the ideal  $(001)_\gamma$  orientation]. This confirms the assumption of a continuous range of orientations extending between two neighbouring KS orientations with an NW orientation in the middle, forming together one (of 12

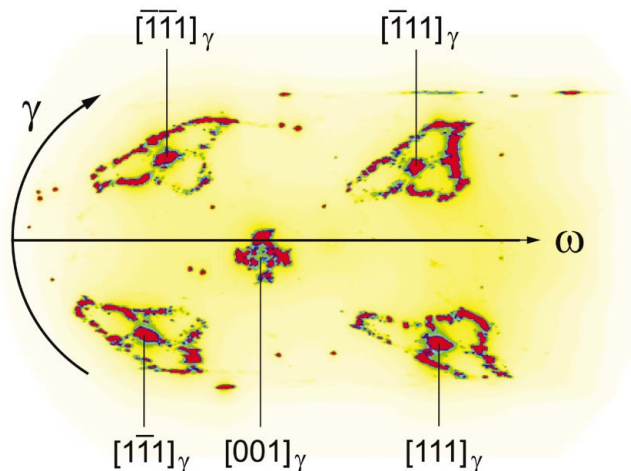


**Figure 3**  
Distribution of  $\langle 110 \rangle$  directions of the kamacite lamellae [ $\langle 110 \rangle$  pole figure] measured with the technique of Fig. 1. The orientation of the sample deviated slightly from the ideal  $(001)_\gamma$  orientation.

symmetrically equivalent) continuous variants of the orientation relationship equation (1).

The symmetrically equivalent branches of Fig. 4(c) are not evenly covered with crystals in Fig. 3. This is attributed to insufficient statistics of kamacite lamellae in the irradiated sample volume. However, no preferred positions between  $KS$  and  $NW$  can be seen, hence corroborating the assumption of continuous variability of orientations between the limiting orientations  $KS_L$  and  $KS_R$ .

The parallelism of planes [left-hand side of equation (1)] shows deviations of the order of  $\mp 1.5^\circ$ . This deviation is beyond the angular resolution of the employed imaging technique, which may be estimated from the size of the ‘stray’ orientations in Fig. 3. Additionally to the orientations expected according to this model, Fig. 3 shows three spread lines around each of the  $\langle 111 \rangle_\gamma$  poles. These are also plotted in Fig. 4(c), as dashed lines. They indicate a ‘transition path’ in the direction of the shortest distance between neighbouring non-coplanar variants.

It may thus be concluded that the parallelism of crystal planes, according to the left-hand side of equation (1), corresponds to an energetic minimum, whereas that of directions [right-hand side of equation (1)] is energetically equal over a rotation angle of  $\sim 10.53^\circ$  and increases only outside this range. Besides that, the crystal plane may relatively easily ‘flip over’ to a neighbouring stable plane orientation, separated by  $\sim 10.53^\circ$ , along a path connecting the respective  $KS$  ends of both non-coplanar variants (the dashed lines in Fig. 4c). Along this path a minimum of orientation density may be seen, thus indicating a moderate energetic maximum in its middle.

It is worth mentioning that the observed continuous orientation variability is not due to a continuous orientation variation inside individual kamacite lamellae of the Widmannstätten structure. Rather, blocks of the order of  $\sim 100 \mu\text{m}$  showed constant orientation within  $\sim 0.5^\circ$ , *i.e.* the experimental accuracy of orientation maps based on electron backscattering patterns (EBSP) patterns. For more details see *e.g.* Schwarzer & Sukkau (2003). Hence, it may be assumed that kamacite lamellae nucleate with orientations that are continuously distributed along the coplanar ranges as well as the non-coplanar transition ranges, but then each of them grows as a virtually perfect crystal with definite grain boundaries separating it from its neighbours.

The transition between the  $NW$  and  $KS$  orientations is thus continuous (graded) in the orientation space but discontinuous in the real space, and there seems to be no correlation between orientation and direct space. This latter question is presently being studied in more detail by automated EBSP techniques.

#### 5. Conclusion

(i) The studied sample of an iron–nickel meteorite consists of kamacite plates, the orientations of which apparently follow very closely the ideal orientation relationship of the  $\gamma \rightarrow \alpha$  transformation at thermal equilibrium.

(ii) Details of this distribution could be well resolved with a high-resolution moving-detector ‘imaging’ technique using diffraction of high-energy synchrotron radiation at the beamline BW5 at HASYLAB/DESY in Hamburg.

(iii) The observed orientation distribution consists of 12 symmetrically equivalent essentially one-dimensional ranges  $\{KS_L-NW-KS_R\}_i$  centred at the 12 Nishiyama–Wassermann (NW) orientations,  $\{110\}_\alpha || \{111\}_\gamma$ ;  $\langle 110 \rangle_\alpha || \langle 112 \rangle_\gamma$ , and extending continuously to both neighbouring Kurdjumov–Sachs (KS) orientations,  $\{110\}_\alpha || \{111\}_\gamma$ ;  $\langle 111 \rangle_\alpha || \langle 110 \rangle_\gamma$ . Hence, these one-dimensional ranges of  $10.53^\circ$  length must be

considered to be the ideal ‘entities’ of the orientation relationship of the  $\gamma \rightarrow \alpha$  transformation rather than the zero-dimensional orientations proposed alternatively by Nishiyama–Wassermann and Kurdjumov–Sachs, respectively.

(iv) The shortest distance in orientation space between two non-coplanar  $\{KS_L-NW-KS_R\}$  ranges is that between their respective KS ends, amounting to  $10.53^\circ$ . A continuous spread of orientations along this line was also observed, though with lower orientation density.

(v) The continuous orientation range is not observed inside the individual kamacite lamellae, which are rather perfect crystals with virtually no orientation gradients in them.

We are indebted to the Mineralogical Museum of the University of Cologne for making a sample of the Gibeon meteorite available for investigation.

### References

- Buchwald, V. F. (1975). *Handbook of Iron Meteorites*. University of California, Berkeley.
- Bunge, H. J., Weislak, L., Klein, H., Garbe, U. & Schneider, R. J. (2002). *Adv. Eng. Mater.* **4**, 300–305.
- Haasen, P. (1974). *Physikalische Metallkunde*. Berlin: Springer Verlag.
- Heide, H. & Wlotzka, K. (1995). *Meteorites*. Berlin: Springer Verlag.
- Höfler, S., Will, G. & Hamm, H. M. (1988). *Earth Planet. Sci. Lett.* **90**, 1–10.
- Kurdjumov, G. & Sachs, G. (1930). *Z. Phys.* **64**, 325–343.
- Mehl, R. F. (1963). *On the Widmannstätten Structure*. In *The Sorby Centennial Symposium on the History of Metallurgy*, edited by C. S. Smith, pp. 245–269. New York: Gordon and Breach.
- Moras, K., Fischer, A., Klein, H. & Bunge, H. J. (2000). *J. Appl. Cryst.* **33**, 1162–1174.
- Nishiyama, Z. (1934). *Sci. Rep. Tohoku Imp. Univ. Tokyo*, **23**, 637–664.
- Schwarzer, R. A. & Sukkau, J. (2003). *Adv. Eng. Mater.* In the press.
- Wassermann, G. (1935). *Mitt. K.-Wilh.-Inst Eisenforsch.* **17**, 149–155.
- Wassermann, G. & Grewen, J. (1962). *Texturen metallischer Werkstoffe*. Berlin: Springer Verlag.
- Weislak, L., Klein, H., Bunge, H. J., Garbe, U., Tschentscher, T. & Schneider, R. J. (2002). *J. Appl. Cryst.* **35**, 82–95.
- Weiss, W. & Bunge, H. J. (2001). *J. Appl. Cryst.* **34**, 566–572.

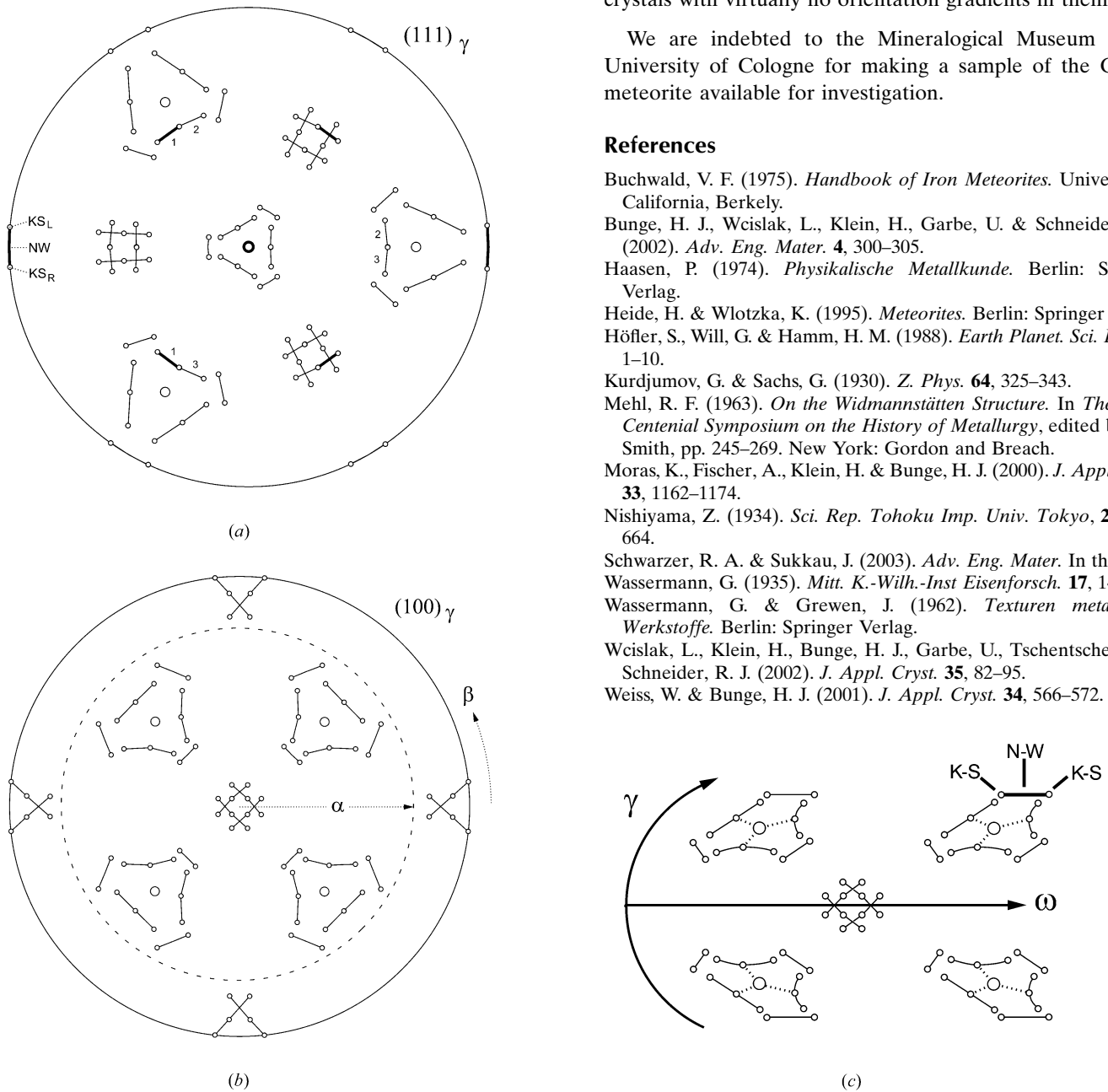


**Figure 4** Distribution of  $\langle 110 \rangle$  directions of kamacite lamellae according to the orientation relationship given by equation (1), assuming a continuous range of orientations from  $KS_L$  to  $KS_R$ , centred at the NW orientation. (a) Projection onto a  $(111)_\gamma$  plane. The three coplanar variants 1, 2, 3 are marked explicitly, one of them by bold lines. (b) Projection onto a  $(100)_\gamma$  plane. The dashed circle corresponds to the visible area of Fig. 3. The conventional polar coordinates  $\{\alpha\beta\}$  are also shown. (c) The area within the dashed circle of (b) transformed to the experimental coordinates  $\{\omega\gamma\}$ . The ‘additional’ spread lines around the central  $[111]_\gamma$  directions of Fig. 3 are also shown by dashed lines.